Dislocations in laser-doped silicon detected by micro-photoluminescence spectroscopy

Hieu T. Nguyen,[a] Young Han, Marco Ernst, Andreas Fell, Evan Franklin, and Daniel Macdonald

Research School of Engineering, College of Engineering and Computer Science, The Australian National University, Canberra ACT 2601, Australia

We report the detection of laser-induced damage in laser-doped layers at the surface of crystalline silicon wafers, via micron-scale photoluminescence spectroscopy. The properties of the sub-band-gap emission from the induced defects are found to match the emission characteristics of dislocations. Courtesy of the high spatial resolution of the micro-photoluminescence spectroscopy technique, micron-scale variations in the extent of damage at the edge of the laser-doped region can be detected, providing a powerful tool to study and optimize laser-doping processes for silicon photovoltaics. © 2015 AIP Publishing LLC. [http://dx.doi.org/10.1063/1.4926360]

Recently, there has been growing interest in employing micro-photoluminescence spectroscopy (μPLS) as a non-destructive and precise characterization tool in silicon photovoltaics (PV). With the advantages of high spatial and spectral resolution, μPLS techniques have been utilized to pinpoint micron-scale features of defects and impurities in crystalline silicon (c-Si), such as Fe precipitates,[1] dislocations,[2–6] or internal stress.[7] Besides that, μPLS has been also employed to extract minority carrier lifetimes around grain boundaries in multicrystalline silicon (mc-Si) wafers,[8] to quantify doping densities in laser-doped regions,[9–12] and to detect very thin localized diffusion layers.[13] On the other hand, laser doping has been demonstrated to be an effective method to create heavily doped regions required for junction and contact formation in high efficiency silicon solar cells.[14–17] Despite the precision and simplicity of laser doping compared to doping techniques such as thermal diffusion or ion implantation, laser doping has been known to induce dislocations in the heavily doped layers, which in turn can have detrimental effects on final cell performance.[18–20] Moreover, a challenge in the characterization of laser-doped regions is the strong spatial non-uniformity on the micron scale, in particular, at potentially highly defective edge regions.[21–23]

In this study, we demonstrate the micron-scale detection of laser-induced dislocations embedded in the highly doped layers using μPLS. We first compare and explain the PL spectra emitted from different regions of laser-doped silicon wafers, including at the edges of the doped regions. We then demonstrate that the observed sub-band-gap PL signal is due to dislocations by comparing its energy position and temperature dependence with those of the well-known dislocation-related "D-lines" from mc-Si wafers. Finally, we also report and explain the observed excitation power dependence of the dislocation PL intensity.

First, we describe the underlying principles of this approach. When illuminated by appropriate excitation wavelengths, silicon wafers with thin heavily doped layers at the surface give rise to two separate peaks in their photoluminescence spectra at low temperatures,[13] courtesy of band-gap narrowing effects in the heavily doped layer.[24,25] On the other hand, dislocations in c-Si are known to emit distinct sub-band-gap PL lines besides the band-to-band (BB) line at low temperatures.[2–6] The laser-doping process can induce structural defects, in particular, dislocations, during the solidification phase of molten silicon.[18–20] Therefore, at low temperatures, PL spectra from laser-doped silicon wafers could be expected to contain three different components originating from three different mechanisms. The first component is emitted by the radiative recombination of free carriers between the two band edges from the underlying silicon substrate, referred to here as SiBB (Silicon Band-to Band). The second component is also band-to-band radiation, but emitted from the thin laser-doped layer, and therefore, subject to a shift to longer wavelengths due to band-gap narrowing effects in this heavily doped layer, referred to as HDBB (heavily doped band-to-band). The third component is due to laser damage caused by the laser-doping process, referred to as LD (laser damage). These three components cannot be distinguished from each other at room temperature, since the SiBB and HDBB lines merge into a very broad peak due to thermal broadening; and the luminescence from dislocations is almost absent since most of the carriers trapped at the defect levels are thermally excited back to their corresponding band edges.[26–29]

A description of the experimental setup of our μPLS system can be found in Refs. 6 and 13. This μPLS system has a spectral resolution of 0.25 nm. The employed excitation sources were a continuous wave 532-nm diode-pumped solid-state (DPSS) laser and an 830-nm laser diode. For both lasers, the on-sample laser spot size was about 1 μm in diameter, and the on-sample excitation power was about 6 mW. The spectral response of the entire system was determined with a calibrated halogen-tungsten light source. The investigated sample was a phosphorus-doped n-type float zone silicon wafer with a background doping level of 7×10^{14} cm^{-3}. It was chemically etched with tetramethylammonium hydroxide (TMAH) solution for 10 min to remove saw damage.

[a]Author to whom correspondence should be addressed. Electronic mail: hieu.nguyen@anu.edu.au

107, 022101-1

The dopant source used for the laser-doping process was a commercial boron spin-on-dopant solution. The laser doping was achieved using a KrF laser having 248-nm wavelength, 3.9-J.cm^{-2} fluence, 25-ns pulse duration, and 320-μm square laser spot size.[17,30] Note that these laser parameters, with a relatively high fluence and a homogenous spot instead of the more typical Gaussian beam shape, are different from those commonly used in silicon solar cell applications. They were used in this case to achieve a moderately high level of damage and a narrow, distinctive edge region, which best illustrates the capabilities of the presented characterization method. A 3D optical surface image of the edge of the investigated laser-doped region is given in Figure 1(a). Due to the high laser fluence, the edge is heavily damaged, giving a very inhomogeneous surface structure. This damaged edge is several microns higher than the wafer surface and about 10-μm wide.

Figure 1(b) plots the normalized PL spectra captured at different locations including the doped, undoped, and the edge (interface between doped and undoped) regions, excited by the 532-nm laser at 79 K. Compared to the undoped region, both the edge and doped regions give rise to a very strong PL peak located around 1270 nm. This peak is due to the damage caused by the laser-doping process. Moreover, at the edge region, this LD peak is so intense that the SiBB peak is completely quenched. Thus, we normalized the spectrum from the edge region to the LD peak, instead of to the SiBB peak. The results suggest that the edge region is much more heavily damaged by the laser doping than the doped region itself, which can have a significant impact on device performance. Figure 1(a) also includes the spectrum from the same location in the doped region, but excited by the 830-nm laser. Since the absorption depth of the 830-nm excitation wavelength is about 45 μm at 79 K, compared to 3 μm for the 532-nm laser (calculated from Ref. 31), most of the 830-nm laser light is absorbed in the silicon substrate. Therefore, the LD peak is nearly absent in the PL spectrum from the doped region when illuminated by the 830-nm laser. This result confirms that the LD peak located around 1270 nm comes from the near-surface region.

As discussed above, at low temperatures, the spectra from the edge and doped regions should contain the HDBB peak associated with the heavily doped layer, due to bandgap narrowing effects in this layer. This HDBB peak is absent in Figure 1(b), since it has been completely masked by the very intense and broad LD peak. However, defect luminescence usually displays a very strong thermal quenching rate, since more carriers trapped at defect levels in the forbidden gap can be thermally activated and return to their nearest band edges with increasing temperatures.[26–29] Hence, as the temperature increases, the LD peak should be suppressed and the HDBB peak may appear. Figure 1(c) shows the change of the spectrum shape from the laser-doped region as the temperature increases, excited by the 532-nm laser. The HDBB peak is clearly revealed at 150 K due to the suppression of the LD peak. At room temperature, the LD peak almost disappears and only a very broad peak located around 1140 nm is present. This broad peak at room temperature is the aggregate PL signal of both the SiBB and HDBB lines.[13] Note that there is also a very sharp peak located at 1064 nm on all spectra. This is not the entirely suppressed 1064-nm component from the 532-nm DPSS laser.

Now, we verify that the LD line is due to dislocations, which are known to be induced by the laser-doping process.[18–20] Dislocations are known to be the underlying cause for four distinct deep-level PL lines, namely, D1, D2, D3, and D4 at low temperatures.[2–6] The D3 and D4 lines have been confirmed to reflect the intrinsic properties of dislocations whereas the D1 and D2 lines have been demonstrated to be emitted by other defects and impurities trapped around dislocation sites.[4–6] Thus, we may expect the LD line to match the D3 and D4 lines.

Figure 2(a) plots the deep-level PL spectrum of dislocations captured at a sub-grain boundary in the mc-Si wafer from Ref. 6 at 79 K. The D4 and D3 lines have their peak locations around 1230 and 1300 nm, respectively. The D4 line's peak location has been shifted by ~100 nm compared to that of the SiBB line. This shift is similar to the shift between the LD and HDBB lines observed here. Note that this particular sub-grain boundary was chosen for comparison as it yielded strong D3 and D4, but very low D1 and D2 emissions (see Ref. 6 for more details on the properties of these D lines). In addition, Figure 2(b) plots the intensities of the D3, D4, and LD lines versus temperature. Each individual line was decomposed from their corresponding spectra using Gaussian functions.[6] The amplitude of each resultant Gaussian function is the peak intensity of its corresponding line. In Figure 2(b), the thermal dependence of the LD line is very similar to that of both D3 and D4 lines. Thus, all three lines should have a similar activation energy E_A, which can
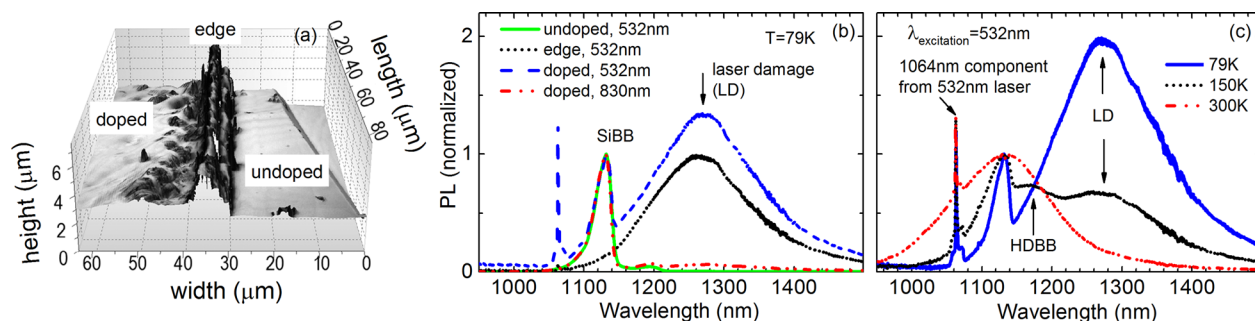

FIG. 1. (a) 3D optical surface image at the edge of the laser-doped region. (b) Normalized PL spectra of the undoped, edge, and doped regions, excited by the 532-nm and 830-nm lasers at 79 K. The spectrum of the edge was normalized to the LD peak, whereas those of the doped and undoped regions were normalized to the SiBB peak. (c) Temperature dependence of normalized PL spectra from the doped region, excited by the 532-nm laser.
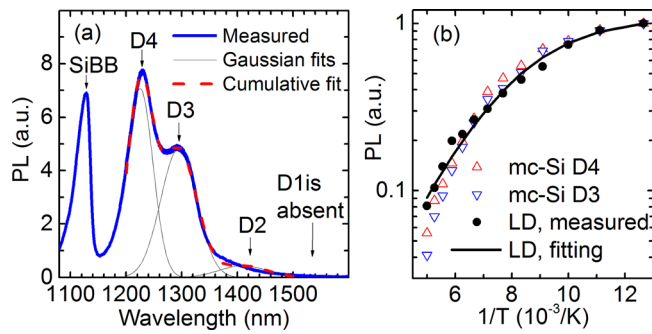
FIG. 2. (a) PL spectrum from dislocations at a sub-grain boundary of a mc-Si wafer, excited by the 532-nm laser at 79 K. (b) Temperature dependence of peak intensities of the LD, D3, and D4 lines, excited by the 532-nm laser.

be extracted by fitting the equation below with the experimental data[26–29]

$$I(T) = \frac{I_0}{1 + CT^{3/2} \exp\left(-\dfrac{E_A}{kT}\right)}, \qquad (1)$$

where $I(T)$ is the PL intensity at a certain absolute temperature T, I_0 is a constant, C is a fitting parameter, and k is Boltzmann's constant. The factor $T^{3/2}$ accounts for the effective density of states in the band edge. The derivation and meaning of these parameters are explained in detail in Ref. 26. Fitting the data in Figure 2(b) gives E_A of 38, 43, and 46 meV for the LD, D4, and D3 lines, respectively, which are within experimental uncertainty. The fitting of Eq. (1) for the LD line is also plotted in Figure 2(b). Note that above 150 K, the slope of the LD line is somewhat lower than that of the D3 and D4 lines. This discrepancy may be explained by the fact that the damage is in the near-surface region whose thickness is only about 1 μm, and the absorption depth of the laser is shorter at higher temperatures. Therefore, more 532-nm laser light is absorbed in the laser-doped region at higher temperatures, contributing more to the relative LD intensity. Meanwhile, for the mc-Si wafer, the dislocation density is expected to be uniform depthwise, and thus, the changing absorption depth is not expected to affect the slopes of D3 and D4 for that sample.

Since the energy difference between LD and HDBB is similar to that between D4 and SiBB, and the activation energy E_A of LD is also similar to that of D4 from dislocations, we conclude that this LD line is emitted by dislocation sites formed during the laser-doping process. The large difference in the full-width at half-maximum (FWHM) between LD and D4 may be explained by two reasons. The first is caused by the fact that the doping profile of the heavily doped layer is not homogeneous depthwise. Therefore, LD is in fact the combined emission from layers of different doping densities, which are shifted by varying amounts due to changing band-gap narrowing, thus leading to a broader peak than D4 emitted from a sample with a homogenous doping density depthwise. Another possibility is that LD may contain components of both D3 and D4, and these two lines are also broadened due to the inhomogeneous doping profile. However, decomposing these two lines from the broad LD line is difficult since the peaks of D3 and D4 in

this case are very broad and not well-defined compared to those of the mc-Si wafer.

Next, we investigate the dependence of the LD line on the excitation power. Figure 3(a) plots the normalized PL spectra from the doped region with various 532-nm excitation powers at 79 K. Similar to the case of diffused silicon wafers,[13] the spectra from the damaged laser-doped region show a strong dependence on the excitation power due to different injection dependencies of the PL signals from the two different layers—the heavily doped layer and the underlying silicon substrate. However, within the heavily doped layer, the HDBB and LD lines also show different injection dependencies from each other due to different recombination mechanisms. The D3 and D4, and thus LD, lines were demonstrated to be emitted by the recombination of trapped carriers between a deep level (E_D) and a shallow level (E_S),[26–29] as illustrated in Figure 3(b). This two-level model is implied from the very strong temperature dependence of D3 and D4, which suggests the participation of shallow levels; and also from the relatively large energy difference between these two lines and the BB line, which suggests the presence of deeper levels. Here, we assume that E_D and E_S are closer to the conduction band (E_C) and the valance band (E_V), respectively. Hence, the energy difference between E_S and E_V is the activation energy E_A in Eq. (1). In case E_D and E_S swap their positions, the following explanation is still valid by simply swapping the roles of electrons and holes.

The radiative recombination rate between the two levels E_D and E_S depends on the product of the number of electrons trapped at E_D and the number of holes trapped at E_S. The occupational probability of electrons at E_D is given by[26,32]

$$f_e(E_D) = \frac{1}{1 + \exp\left(\dfrac{E_D - E_{FC}}{kT}\right)}, \qquad (2)$$

with E_{FC} being the quasi-Fermi level of electrons under illumination.

The number of free electrons located around the defect centers is determined by[32]

$$n_e = N_C \exp\left(\frac{E_{FC} - E_C}{kT}\right), \qquad (3)$$
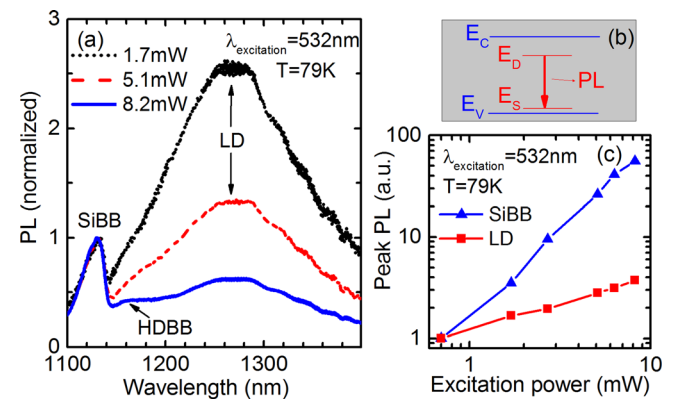

FIG. 3. (a) Excitation power dependence of normalized PL spectra from the laser-doped region, excited by the 532-nm laser at 79 K. (b) Illustration for the recombination scheme of deep-level PL. (c) Peak intensities of the LD and SiBB lines versus 532-nm excitation power at 79 K.

where N_C is the effective density of states in the conduction band.

Combining Eqs. (2) and (3) yields

$$f_e(E_D) = \frac{1}{1 + \dfrac{N_C}{n_e} \exp\left(\dfrac{E_D - E_C}{kT}\right)}. \qquad (4)$$

N_C and kT are $\sim 4 \times 10^{18}\,\text{cm}^{-3}$ and $\sim 7\,\text{meV}$ at 79 K, respectively. Under high injection, $n_e \approx \Delta n$, which is the excess carrier density and is estimated to be about 10^{17}–$10^{18}\,\text{cm}^{-3}$. Since $E_C - E_D$ is much higher than kT at 79 K, the second term in the denominator of Eq. (4) is much less than 1. Therefore, the occupational probability of electrons at E_D is independent of Δn under high injection at low temperatures.[26] With the same derivation for holes, the occupational probability of holes at E_S still slightly depends on Δn. The boundary occurs when E_S approaches E_V, in which case the occupational probability linearly depends on Δn. As a result, the radiative recombination rate via the defect centers does not increase as fast as Δn.

Meanwhile, the BB recombination rate is determined by $\Delta n \times (\Delta n + N_D)$.[33] Hence, the SiBB peak intensity is a quadratic function of Δn in high injection, but the HDBB peak intensity is still between a linear and quadratic function of Δn. Therefore, the LD line is reduced most quickly with increasing excitation power when the spectra are normalized relative to the BB peak, as in Figure 3(a). Note that the HDBB line is eventually revealed with increasing excitation power in Figure 3(a) due to its intermediate dependence on Δn.

In order to fortify the explanation above, Figure 3(c) plots the peak intensities of the SiBB and LD lines versus the excitation power in logarithmic scale. In order to avoid overlapping the two lines, the data of the LD line were captured at the edge of the laser-doped region (the SiBB line was absent), and those of the SiBB line were captured at the undoped region (only the SiBB line was present). The slope of the SiBB curve is close to 2 since the SiBB PL signal is proportional to Δn^2 under high injection, but that of the LD curve is significantly less than 1. The results from this figure are, therefore, consistent with the explanation of different recombination mechanisms between the SiBB and LD lines above. We note that, in general, different laser-doping techniques or conditions may give rise to different types of defect luminescence.

In summary, micro-photoluminescence spectroscopy has been applied to detect laser-induced damage in heavily doped layers of laser-doped crystalline silicon wafers for solar cell applications. The high spatial resolution of this method can be of particular use to identify defective edge regions which impact device performance. The detected laser-induced damage is demonstrated to be caused by dislocations, due to the similar properties of its PL spectrum compared to those of dislocations. This method is effective for probing micron-scale features of laser-doped regions and could be employed as a characterization tool for studying and optimizing laser-doping processes for silicon photovoltaics.

[1]P. Gundel, M. C. Schubert, W. Kwapil, J. Schön, M. Reiche, H. Savin, M. Yli-Koski, J. A. Sans, G. Martinez-Criado, W. Seifert, W. Warta, and E. R. Weber, Phys. Status. Solidi RRL **3**, 230 (2009).
[2]T. Sekiguchi and K. Sumino, J. Appl. Phys. **79**, 3253 (1996).
[3]W. Lee, J. Chen, B. Chen, J. Chang, and T. Sekiguchi, Appl. Phys. Lett. **94**, 112103 (2009).
[4]M. Tajima, Y. Iwata, F. Okayama, H. Toyota, H. Onodera, and T. Sekiguchi, J. Appl. Phys. **111**, 113523 (2012).
[5]M. Tajima, IEEE J. Photovoltaics **4**, 1452 (2014).
[6]H. T. Nguyen, F. E. Rougieux, F. Wang, H. Tan, and D. Macdonald, IEEE J. Photovoltaics **5**, 799 (2015).
[7]P. Gundel, M. C. Schubert, and W. Warta, Phys. Status Solidi A **207**, 436 (2010).
[8]P. Gundel, F. D. Heinz, M. C. Schubert, J. A. Giesecke, and W. Warta, J. Appl. Phys. **108**, 033705 (2010).
[9]R. Woehl, P. Gundel, J. Krause, K. Rühle, F. D. Heinz, M. Rauer, C. Schmiga, M. C. Schubert, W. Warta, and D. Biro, IEEE Trans. Electron Devices **58**, 441 (2011).
[10]P. Gundel, D. Suwito, U. Jäger, F. D. Heinz, W. Warta, and M. C. Schubert, IEEE Trans. Electron Devices **58**, 2874 (2011).
[11]F. D. Heinz, P. Gundel, W. Warta, and M. C. Schubert, IEEE J. Photovoltaics **3**, 341 (2013).
[12]A. Roige, J. Alvarez, J.-P. Kleider, I. Martin, R. Alcubilla, and L. F. Vega, IEEE J. Photovoltaics **5**, 545 (2015).
[13]H. T. Nguyen, D. Yan, F. Wang, P. Zheng, Y. Han, and D. Macdonald, Phys. Status Solidi RRL **9**, 230 (2015).
[14]E. Schneiderlöchner, R. Preu, R. Lüdemann, and S. W. Glunz, Prog. Photovoltaics Res. Appl. **10**, 29 (2002).
[15]D. Kray, A. Fell, S. Hopman, K. Mayer, G. P. Willeke, and S. W. Glunz, Appl. Phys. A **93**, 99 (2008).
[16]E. Franklin, K. Fong, K. McIntosh, A. Fell, A. Blakers, T. Kho, D. Walter, D. Wang, N. Zin, M. Stocks, E. C. Wang, N. Grant, Y. Wan, Y. Yang, X. Zhang, Z. Feng, and P. J. Verlinden, "Design, fabrication and characterisation of a 24.4% efficient interdigitated back contact solar cell," Prog. Photovoltaics Res. Appl. (published online).
[17]M. Dahlinger, B. Bazer-Bachi, T. C. Röder, J. R. Köhler, R. Zapf-Gottwick, and J. H. Werner, IEEE J. Photovoltaics **5**, 812 (2015).
[18]A. Sugianto, B. S. Tjahjono, J. H. Guo, and S. R. Wenham, "Impact of laser induced defects on the performance of solar cells using localised laser doped regions beneath the metal contacts," in 22nd European Photovoltaic Solar Energy Conference, Milan, Italy (2007).
[19]S. Hopman, A. Fell, K. Mayer, C. Fleischmann, K. Drew, D. Kray, and F. Granek, "Study on laser parameters for silicon solar cells with LCP selective emitters," in *24th European Photovoltaic Solar Energy Conference and Exhibition, Hamburg, Germany* (2009).
[20]Z. Hameiri, T. Puzzer, L. Mai, A. B. Sproul, and S. R. Wenham, Prog. Photovoltaics Res. Appl. **19**, 391 (2011).
[21]X. Lujia, K. Weber, A. Fell, Z. Hameiri, P. Sieu Pheng, Y. Xinbo, and E. Franklin, IEEE J. Photovoltaics **4**, 594 (2014).
[22]A. Fell, S. Surve, E. Franklin, and K. J. Weber, IEEE Trans. Electron Devices **61**, 1943 (2014).
[23]C. Geisler, W. Hördt, S. Kluska, A. Mondon, S. Hopman, and M. Glatthaar, Sol. Energy Mater. Sol. Cells **133**, 48 (2015).
[24]J. Wagner, Phys. Rev. B **29**, 2002 (1984).
[25]J. Wagner, Phys. Rev. B **32**, 1323 (1985).
[26]M. Suezawa, Y. Sasaki, and K. Sumino, Phys. Status Solidi A **79**, 173 (1983).
[27]R. Sauer, J. Weber, J. Stolz, E. R. Weber, K.-H. Küsters, and H. Alexander, Appl. Phys. A **36**, 1 (1985).
[28]V. V. Kveder, E. A. Steinman, S. A. Shevchenko, and H. G. Grimmeiss, Phys. Rev. B **51**, 10520 (1995).

[29]M. C. Schubert, P. Gundel, M. The, W. Warta, M. Romero, S. Ostapenko, and Tz. Arguirov, "Spatially resolved luminescence spectroscopy on multicrystalline silicon," in *Proceedings of 23rd EU-PVSEC, Valencia* (2008), p. 17.

[30]D. Walter, A. Fell, E. Franklin, D. Wang, K. Fong, T. Kho, K. Weber, and A. W. Blakers, Sol. Energy Mater. Sol. Cells **136**, 1 (2015).

[31]M. A. Green, Sol. Energy Mater. Sol. Cells **92**, 1305 (2008).

[32]P. Würfel, *Physics of Solar Cells: From Basic Principles to Advanced Concepts* (Wiley-VCH, 2009), p. 81.

[33]H. T. Nguyen, F. E. Rougieux, S. C. Baker-Finch, and D. Macdonald, IEEE J. Photovoltaics **5**, 77 (2015).